HYBRID POWER FLOW ANALYSIS USING SEA PARAMETERS

Y.-H. PARK and S.-Y. HONG*

Seoul National University, Development of Naval Architecture & Ocean Engineering, Seoul 151-742, Korea

ABSTRACT–This paper proposes a hybrid analytic method for the prediction of vibrational and acoustic responses of reverberant system in the medium-to-high frequency ranges by using the PFA (Power Flow Analysis) algorithm and SEA (Statistical Energy Analysis) coupling concepts. The main part of this method is the application of the coupling loss factor (CLF) of SEA to the boundary condition of PFA in reverberant system. The hybrid method developed shows much more promising results than the conventional SEA and equivalent results to the classical PFA for various damping loss factors in a wide range of frequencies. Additionally, this paper presents applied results of hybrid power flow finite element method (hybrid PFFEM) by formulating the new joint element matrix with CLF to analyze the vibrational responses of built-up structures. Finally, the analytic results of coupled plate structures and an automobile-shaped structure using hybrid PFFEM were predicted successively.

KEY WORDS : Power flow analysis, Statistical energy analysis, Coupling loss factor, Power flow finite element method, Reverberance factor, Hybrid power flow finite element method

1. INTRODUCTION

Recently, as vehicle structures have gradually decreased in weight and increased in speed, there has been an increase in the concern for structural/acoustic dynamic responses in the medium-to-high frequency ranges. Much of the current structural vibration analyses have been done by using the traditional finite element method (FEM). However, to properly model high-frequency vibrations, the order of the shape functions in FEM must be increased or the size of the mesh decreased. Therefore, traditional finite element models are disadvantageous to performing accurate high-frequency analysis because they become too large for efficient application (Wohlever and Bernhard, 1992).

Additionally, the FEM is essentially a deterministic analysis technique. The method requires all the data for a problem to be known exactly. At low frequencies, the data such as material properties and joint behavior are reasonably well known and the solution is not highly sensitive to typical variations of these data. However, at high frequencies, the required data for structural dynamic problems are uncertain, and thus, the solution is highly sensitive to data variations. Therefore, at high frequencies, the statistical approach for analyzing structural and acoustic responses is more appropriate than

the deterministic one.

Statistical Energy Analysis (SEA) has become a widely accepted technique for modeling dynamic responses of vibro-acoustic systems of high modal density. In SEA, each component of a built-up system is treated as a statistical population of mode groups and the average dynamic response of component parts is calculated (Lyon and Dejong, 1995). Therefore, the analytic model for SEA compared with that for a common FEA is very simple. However, because assumptions are simplified in the development of SEA, the analytic results are not sufficiently reliable in the low-to-medium frequency ranges. Additionally, SEA gives no information about the spatial distribution of dynamic responses within a given subsystem.

Power Flow Analysis (PFA) has been understood to be one of reliable methods, and has remarkable advantages compared to other analytic tools for acoustic and vibrational analysis in the medium-to-high frequency ranges. PFA models the flow of mechanical energy in a manner analogous to the flow of thermal energy in heat conduction. Because the energy governing equation is partial differential equation on space, PFA can give information about the spatial variation of energy density as well as intensity (Cho, 1993).

Power Flow Finite Element Method (PFFEM) is a numerical analytic tool which applies finite element technique to PFA for the vibrational analysis of built-up structures in the medium-to-high frequency ranges.

Corresponding author. e-mail: syh@snu.ac.kr

PFFEM can be effectively used to analyze vibrational and acoustic responses of built-up structures with sufficiently coarse mesh compared with the FEM at high freqneucies (Manning, 2005; Zhang et al., 2005). Additionally, PFFEM has been lately used for the design optimization using PFA at high frequencies (Chuang et al., 2005).

As many researchers have developed SEA since 1959, SEA has much information, especially about the coupling data, which is very important in the analysis of built-up structures and has some commercialized softwares/hardwares calculating SEA parameters. This coupling information can be used efficiently in an alternative method based on energy. In particular, the commercialized NVH software based on energy must support the functions that simulate with the use of experimental parameters to increase the accuracy of analytic results. In this case, the coupling loss factor (CLF) of SEA, which is easier to be obtained, can be used as very efficient information. In relation to these, Langley showed a simple methodology which uses CLF in PFA boundary condition about one kind of motion in a two-dimensional structure for the different object (Langley, 1995).

In this paper, the general algorithm for the use of CLF in PFA boundary condition is presented. Formulation using CLF in PFA boundary condition was developed to cover the all degrees-of-freedom of one-, two-, and three-dimensional cases, and was proven to be valid through numerical analyses of each dimensional case. Additionally, the new joint element matrix using CLF for the Power Flow Finite Element Method (PFFEM) was developed to extend the application area of the developed hybrid method to built-up structures. To verify its validity and accuracy, numerical analyses of coupled plate structures were performed in various conditions. Finally, using the developed hybrid PFFEM, the numerical applications for a simple automobile-shaped structure were represented.

2. FORMULATION OF HYBRID BOUNDARY CONDITION IN POWER FLOW ANALYSIS

2.1. One-dimensional Case

The equation of motion for the uniform Bernoulli-Euler beam excited by a transverse harmonic point force is

$$E_c I \frac{\partial^4 w}{\partial x^4} + \rho S \frac{\partial^2 w}{\partial t^2} = F \delta(x - x_0) e^{j\omega t}, \qquad (1)$$

where $E_c = E(1 + j\eta)$ is the complex modulus of elasticity, I is the moment of inertia, ρ is the density, S is the sectional area, w is the transverse displacement, η is the hysteretic damping loss factor and F is the harmonic flexural point force applied at point x_0. The general solution of equation (1) is

$$w(x, t) = (A e^{-jk_c x} + B e^{-jk_c x} + C e^{-k_c x} + D e^{k_c x}) e^{j\omega t}, \qquad (2)$$

where is the complex wave number defined by the expression

$$k_c = \sqrt[4]{\left(\frac{\omega}{c_b}\right) \frac{(1 - j\eta)}{(1 + \eta^2)}}, \qquad (3)$$

in which $c_b = \sqrt[4]{\omega^2 EI / \rho S}$ is the phase velocity of flexural wave in the beam.

Goyder et al. (1980) have shown that the far-field component of energy and power by transverse displacement in equation (2) is dominant to the near-field component at high frequencies. Therefore, in lightly damped structures, i.e., $\eta \ll 1$, if near-field terms of transverse displacement are neglected, the relationship between the time- and locally space-averaged "m"-type far-field energy density and power can be approximated by (Wohlever and Bernhard, 1988)

$$q = \frac{c_{gm}^2}{\eta \omega} \frac{d \langle e \rangle_m}{dx} (m = f, l), \qquad (4)$$

where abbreviations "f" and "l" denote flexural and longitudinal wave respectively.

By the principle of energy conservation in steady state, the energy governing equation which takes the time- and locally space-averaged "m"-type far-field total energy density as a primary variable can be derived by (Wohlever et al., 1992)

$$\frac{c_{gm}^2}{\eta \omega} \frac{d^2 \langle e \rangle_m}{dx^2} + \eta \omega \langle e \rangle_m = \Pi_{in, m} (m = f, l), \qquad (5)$$

where $\Pi_{in, m}$ is the input power of "m"-type wave, $c_{gf} = 2 (\omega^2 EI / \rho S)^{1/4}$ and $c_{gl} = \sqrt{E / \rho}$. The general solution of equation (2.5) is represented as

$$\langle e \rangle_m = A \times \exp(-\psi_m x) + B \times \exp(\psi_m x), \qquad (6)$$

where $\psi_m = \eta \omega / c_{gm}$. In equation (6), the time- and locally space-averaged far-field energy density solution is composed of not propagating wave components but exponentially decaying wave components. Additionally, the value of ψ_m in equation (6) implies the decay rate of "m"-type energy density per unit length. Therefore, the reverberance factor ($\Re_m = \psi_m L$) of "m"-type wave field in a subsystem can be expressed by multiplied by the characteristic length (L) of the subsystem and is related to the exciting frequency, group velocity and characteristic length besides damping loss factor of the subsystem. If the reverberance factor $\Re_m$ of the subsystem is zero, the "m"-type wave field of the subsystem is completely reverberant ($\langle e \rangle_m =$ constant).

Generally, if the hysteretic damping of a structural subsystem is very small ($\eta \ll 1$) like that of the metal, the size of a subsystem is not very large, and the exciting frequency is not very high, energy density will vary slightly within the subsystem. Therefore, except the

subsystem which external force is loaded in this case, the assumption that the energy density in a subsystem is constant, that is reverberant, will not be unreasonable.

Here, if the energy density field in each beam is assumed to be reverberant and the system contains a modal overlap, the power which is transferred from the energy of "m"-type waves in beam 1 to "n"-type waves in beam 2 can be expressed as

$$\Pi_{1m \to 2n} = \omega \eta_{12mn} E_{1m} = \omega \eta_{12mn} L_1 \langle e \rangle_{1m}, \qquad (7)$$

where η_{12mn} is the coupling loss factor from the energy of "m"-type wave in beam 1 to the energy of "n"-type wave in beam 2, E_{1m} is the total energy (J), $\langle e \rangle_{1m}$ is the energy density (J/m) of an "m"-type wave in beam 1, and L_1 is the length of beam 1. The coupling loss factor of point junction in equation (7) is known as

$$\eta_{12mn} = \frac{c_{g1m} \langle \tau \rangle_{12mn}}{2 \omega L_1}, \qquad (8)$$

where c_{g1m} is the group velocity of "m"-type wave in beam 1 and $\langle \tau \rangle_{12mn}$ is the diffuse power transmission coefficient of "n"-type wave in beam 2 due to the incident "m"-type wave in beam 1. By equations (4) and (8), the net power of a "m"-type wave may be represented as

$$\Pi_{1m2n} = \frac{c_{g1m}^2}{\eta_1 \omega} \frac{d \langle e_1 \rangle_m}{dx} = \sum_{n = f, l} (\Pi_{1m \to 2n} - \Pi_{2n \to 1m})$$

$$= \sum_{n = f, l} \omega (L_1 \eta_{12mn} \langle e_1 \rangle_m - L_2 \eta_{21mn} \langle e_2 \rangle_n) \quad \text{and} \qquad (9)$$

$$\Pi_{1n2m} = \frac{c_{g2m}^2}{\eta_1 \omega} \frac{d \langle e_2 \rangle_m}{dx} = \sum_{n = f, l} (\Pi_{1n \to 2m} - \Pi_{2m \to 1n})$$

$$= \sum_{n = f, l} \omega (L_1 \eta_{12mn} \langle e_1 \rangle_n - L_2 \eta_{21mn} \langle e_2 \rangle_m) \qquad (10)$$

The upper equations (9) and (10) represent the hybrid boundary condition mixing the concept of power flow analysis with that of statistical energy analysis, using the power transfer relation in reverberant field. That is to say, using the advantages of each method, the concept of power flow analysis such as equation (5) is used within the homogeneous domain and that of statistical energy
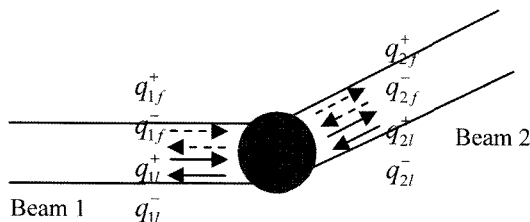

Figure 1. Power flow model for two beams joined at an arbitrary angle.

analysis such as equations (7)~(10) in the boundary.

However, if the hysteretic damping of a structural subsystem is not small, the size of a subsystem is very large, or the exciting frequency is very high, the energy density in its subsystem will vary greatly and its field will be not reverberant any more due to large reverberance factor. In this case, the energy density and power values in the boundary cannot represent those averaged in the full subsystem. Therefore, the hybrid boundary condition at the joint of these highly damped structures may generate more error than the classical boundary condition. In a general field, the classical boundary condition in power flow analysis fully using the power transmission and reflection coefficients derived by wave transmission approach is expressed as follows

$$\langle q \rangle_{2f}^+ = \langle \tau_{12ff} \rangle \langle q \rangle_{1f}^+ + \langle \gamma_{22ff} \rangle \langle q \rangle_{2f}^- + \langle \tau_{12lf} \rangle \langle q \rangle_{1l}^+ + \langle \gamma_{22lf} \rangle \langle q \rangle_{2l}^-,$$

$$\langle q \rangle_{1f}^- = \langle \gamma_{11ff} \rangle \langle q \rangle_{1f}^+ + \langle \tau_{21ff} \rangle \langle q \rangle_{2f}^- + \langle \gamma_{11lf} \rangle \langle q \rangle_{1l}^+ + \langle \tau_{21lf} \rangle \langle q \rangle_{2l}^-,$$

$$\langle q \rangle_{2l}^+ = \langle \tau_{12fl} \rangle \langle q \rangle_{1f}^+ + \langle \gamma_{22fl} \rangle \langle q \rangle_{2f}^- + \langle \tau_{12ll} \rangle \langle q \rangle_{1l}^+ + \langle \gamma_{22ll} \rangle \langle q \rangle_{2l}^-$$
and

$$\langle q \rangle_{1l}^- = \langle \gamma_{11fl} \rangle \langle q \rangle_{1f}^+ + \langle \tau_{21fl} \rangle \langle q \rangle_{2f}^- + \langle \gamma_{11ll} \rangle \langle q \rangle_{1l}^+ + \langle \tau_{21ll} \rangle \langle q \rangle_{2l}^-, \qquad (11)$$

where $\langle q \rangle_f^+$ and $\langle q \rangle_l^+$ are the flexural and longitudinal powers in the positive direction, respectively, and all the powers are the values in the boundary.

Numerical examples
To verify the usefulness of the new hybrid boundary condition on one-dimensional problem, this boundary condition was numerically applied to three finite beams joined at arbitrary angles as shown in Figure 2. To consider the arbitrary case, the dimensions of beams are 2 m × 0.01m × 0.01m, 2m × 0.03m × 0.03m and 2m × 0.03m × 0.03m ($L \times B \times H$) respectively. Beams 1 and 2 are made of steel and beam 3 of aluminum. The angle θ_1 between beams 1 and 2 was assumed to be 45° and θ_2 between beams 2 and 3 to be −45°. The magnitude of the applied transverse point force in the center of incident beam is 100N. The time-averaged input power can be calculated as follows:

$$\Pi_{in} = \frac{1}{2} \text{Re} \left\{ (F e^{j\omega t}) \times \left(\frac{\partial w(x_0)}{\partial t} \right)^* \right\}, \qquad (12)$$

where $w(x_0)$ is the transverse displacement at the loading point.

For the first model, the hysteretic damping values of all beams were assumed to be $\eta = 0.1$. For the second model, to consider the effect of reverberance factors, the structural damping values of all beams were changed into $\eta = 0.001$ corresponding to the value of common
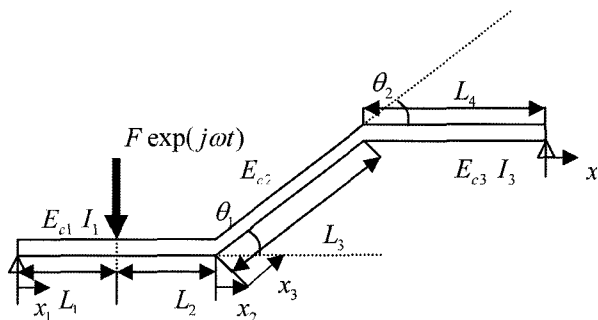
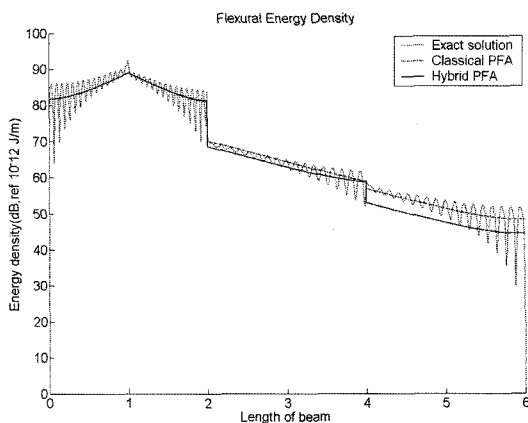Figure 2. Three finite beams jointed at arbitrary angles.

Figure 3. Flexural energy density distribution of first model when $f = 5$ kHz and $\eta = 0.1$ ($\Re_{f1}=4.67$, $\Re_{f2}=2.69$, $\Re_{f3}=2.67$). '——', hybrid PFA solution; '----', classical PFA solution; '······', exact solution.

Figure 4. Longitudinal energy density distribution of first model when and $\eta=0.1$ ($\Re_{f1}=1.26$, $\Re_{f2}=1.26$, $\Re_{f3}= 1.23$). '——', hybrid PFA solution; '----', classical PFA solution; '······', exact solution.

Figure 5. Flexural power distribution of first model when and $\eta=0.1$ ($\Re_{f1}=4.67$, $\Re_{f2}=2.69$, $\Re_{f3}=2.67$). '——', hybrid PFA method; '----', classical PFA solution; '······', exact solution.

metals. The detailed procedure of numerical analysis for the one-dimensional case is discussed in Appendix 1.

Figures 3–6 show the numerical results that are obtained using each boundary condition in all joints for 1/3 octave band with for the first model. In this model, the reverberance factors of flexural and longitudinal wave fields in each beam are $\Re_{f1}=4.67$, $\Re_{f2}=2.69$, $\Re_{f3}= 2.67$, $\Re_{l1}=1.26$, $\Re_{l2}=1.26$, and $\Re_{l3}=1.23$, respectively. As expected, the flexural energy density of exact solution decreases universally with increasing distance from the excitation location and fluctuates locally in space, especially near the ends of the beams and the junction in Figure 3. The flexural energy density of power flow solutions, which are obtained using the classical and hybrid boundary conditions at the joints, varies smoothly in space without any fluctuation and has a discontinuity line at the junction. The exact solutions fluctuate in the vicinity of the smoothed results of the power flow solutions obtained by using the classical and hybrid boundary conditions. The results of power flow solutions, which are obtained by using the classical and hybrid boundary conditions, nearly agree with those of the exact
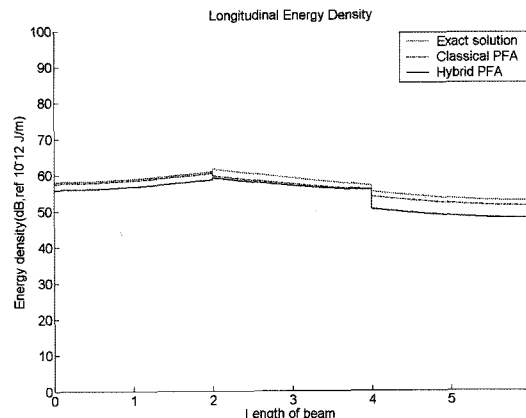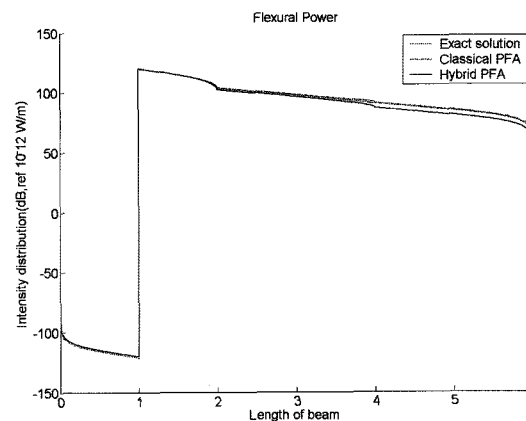
solutions. However, because of large structural damping value ($\eta=0.1$), the difference between results that were obtained by using the classical and hybrid boundary conditions increases as the distance from the excitation location increases. This tendency in the results is also true for the flexural energy as well as the longitudinal energy (Figure 4), the flexural power (Figure 5) and the longitudinal power (Figure 6).

For the second model, Figures 7 and 8 show the numerical results of classical power flow solutions, hybrid power flow solutions, and classical SEA solutions, which are obtained by using each boundary condition in all joints for 1/3 octave band with $f_c=5$ kHz and $\eta=0.001$. The reverberance factors of each wave field in the second model are one hundred times as small as those in the first model due to small damping loss factor.
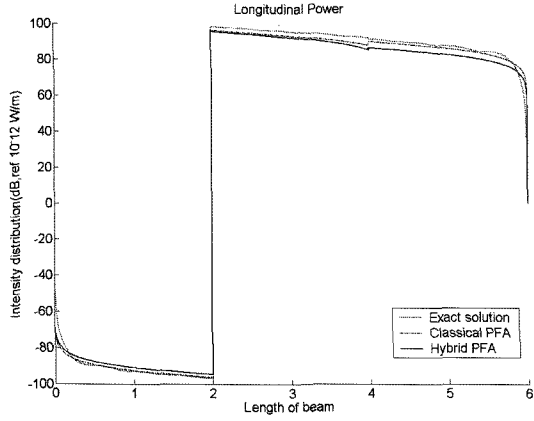
Figure 6. Longitudinal power distribution of first model when $f=5$ kHz and $\eta=0.1$ ($\Re_{f1}=1.26$, $\Re_{f2}=1.26$, $\Re_{f3}=1.23$). '——', hybrid PFA solution; '- - - -', classical PFA solution; '·······', exact solution.

Figure 8. Longitudinal energy density distribution of first model when $f=5$ kHz and $\eta=0.001$ ($\Re_{f1}=0.0126$, $\Re_{f2}=0.0126$, $\Re_{f3}=0.0123$). '——', hybrid PFA solution; '- - - -', classical PFA solution; '·······', classical SEA solution.
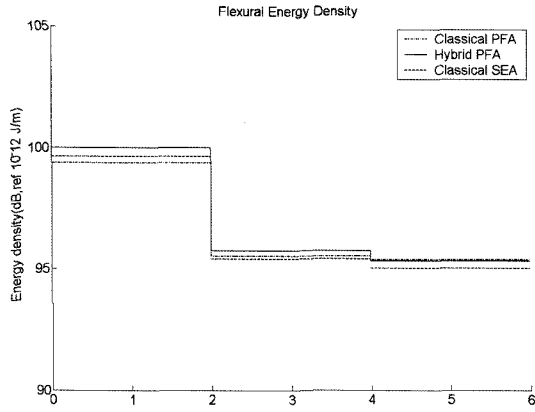
Figure 7. Flexural energy density distribution of first model when $f=5$ kHz and $\eta=0.001$ ($\Re_{f1}=0.0467$, $\Re_{f2}=0.0269$, $\Re_{f3}=0.0267$). '——', hybrid PFA solution; '- - - -', classical PFA solution; '·······', SEA solution.

Because the hybrid boundary condition is equivalent to the classical boundary condition when $\eta=0$ ($\Re_m=0$), the power flow solutions that are obtained using the hybrid boundary condition, become equal to those that are obtained by using the classical boundary condition, as the reverberance factor $\Re_m$ decreases. Corresponding to these expectations, Figures 7 and 8 show that the results that are obtained by using two boundary conditions agree well because the reverberance factors of this model became smaller.

To confirming these results, Figures 9 and 10 show the effects of reverberance factors in flexural and longitudinal energy densities using each boundary condition. The relative differences in the results shown in Figures 9 and 10 are the values of the difference between the averaged energy density using the classical boundary
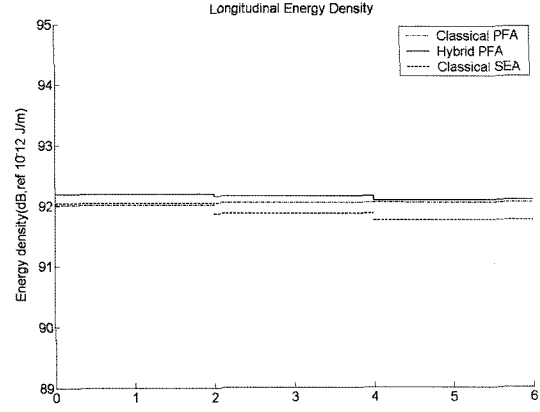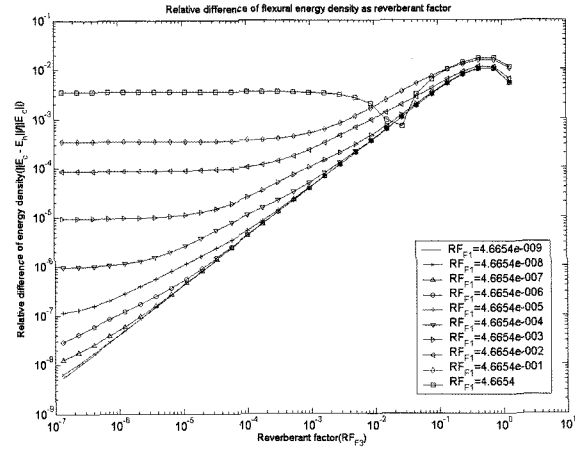

Figure 9. Relative difference ($\|\bar{E}_c - \bar{E}_h\| / \|\bar{E}_c\|$) of space-averaged flexural energy densities by two methods in beam 3 as the reverberance factor variation of beam 1. '——', $\Re_{f1}=4.67 \times 10^{-9}$, '-×-'; $\Re_{f1}=4.67 \times 10^{-8}$; '-△-', $\Re_{f1}=4.67 \times 10^{-7}$; '-○-', $\Re_{f1}=4.67 \times 10^{-6}$; '-|-', $\Re_{f1}=4.67 \times 10^{-5}$; '-▽-', $\Re_{f1}=4.67 \times 10^{-4}$; '-▷-', $\Re_{f1}=4.67 \times 10^{-3}$; '-◁-', $\Re_{f1}=4.67 \times 10^{-2}$; '-◇-', $\Re_{f1}=4.67 \times 10^{-1}$; '-□-', $\Re_{f1}=4.67$.

condition and hybrid boundary condition, divided by the averaged energy density using classical boundary condition ($\|\bar{E}_{3,classic} - \bar{E}_{3,hybrid}\| / \|\bar{E}_{3,classic}\|$) in beam 3.

As expected, the relative differences of energy densities using two boundary conditions approaches zero as the reverberance factors decrease. Therefore, if the reverberance factor of a subsystem is small, the power flow analysis using the hybrid boundary condition will be effective.
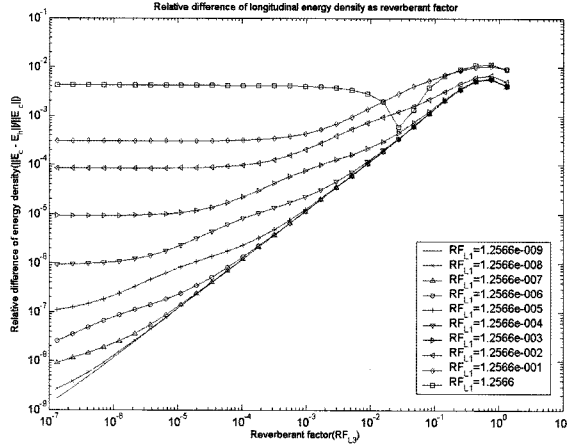
Figure 10. Relative difference ($\|\overline{E}_c - \overline{E}_h\| / |\overline{E}_c|$) of space-averaged longitudinal energy densities by two methods in beam 3 as the reverberance factor variation of beam 1. '——', $\Re_{f1}=1.26 \times 10^{-9}$, '–×–'; $\Re_{f1}=1.26 \times 10^{-8}$; '–△–', $\Re_{f1}=1.26 \times 10^{-7}$; '–○–', $\Re_{f1}=1.26 \times 10^{-6}$; '–|–', $\Re_{f1}=1.26 \times 10^{-5}$; '–▽–', $\Re_{f1}=1.26 \times 10^{-4}$; '–▷–', $\Re_{f1}=1.26 \times 10^{-3}$; '–◁–', $\Re_{f1}=1.26 \times 10^{-2}$; '–◇–', $\Re_{f1}=1.26 \times 10^{-1}$; '–□–', $\Re_{f1}=1.26$.

2.2. Two-dimensional Case

Two-dimensional case obtained by expanding the hybrid algorithm of one-dimensional case will be considered. As an example of two-dimensional case, the energy governing equations of flexural, longitudinal, and shear waves in a thin homogeneous finite plate are expressed, respectively (Park et al., 2001).

$$-\frac{c_{gm}^2}{\eta\omega}\nabla^2\langle e\rangle_m + \eta\omega\langle e\rangle_m = 0 \quad (m= f, l, s), \tag{13}$$

where ∇^2 means two-dimensional Laplace operator.

For each wave in the plate, the relationship of the time- and locally space-averaged far-field total energy density
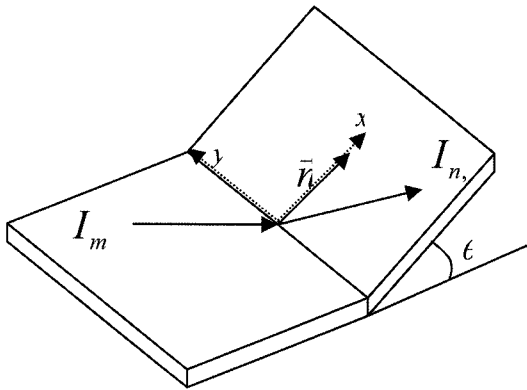

Figure 11. Power flow model for two plates coupled at an arbitrary angle

and intensity using the similar algorithm can be represented as

$$\langle \vec{q}\rangle_m = \frac{c_{gm}^2}{\eta\omega}\left(\frac{\partial}{\partial x}\vec{i} + \frac{\partial}{\partial y}\vec{j}\right)\langle e\rangle_m \quad (m= f, l, s). \tag{14}$$

In the classical power flow analysis, the boundary conditions expressed by diffuse power transmission and reflection coefficients and intensity values in the joint of the model shown in Figure 11, can be written as

$$\langle q_{1x}\rangle_f^- = \langle\gamma_{11ff}\rangle\langle q_{1x}\rangle_f^+ + \langle\gamma_{11lf}\rangle\langle q_{1x}\rangle_l^+ + \langle\gamma_{11sf}\rangle\langle q_{1x}\rangle_s^+$$
$$+ \langle\tau_{21ff}\rangle\langle q_{2x}\rangle_f^- + \langle\tau_{21lf}\rangle\langle q_{2x}\rangle_l^- + \langle\tau_{21sf}\rangle\langle q_{2x}\rangle_s^-,$$

$$\langle q_{1x}\rangle_l^- = \langle\gamma_{11fl}\rangle\langle q_{1x}\rangle_f^+ + \langle\gamma_{11ll}\rangle\langle q_{1x}\rangle_l^+ + \langle\gamma_{11sl}\rangle\langle q_{1x}\rangle_s^+$$
$$+ \langle\tau_{21fl}\rangle\langle q_{2x}\rangle_f^- + \langle\tau_{21ll}\rangle\langle q_{2x}\rangle_l^- + \langle\tau_{21sl}\rangle\langle q_{2x}\rangle_s^-,$$

$$\langle q_{1x}\rangle_s^- = \langle\gamma_{11fs}\rangle\langle q_{1x}\rangle_f^+ + \langle\gamma_{11ls}\rangle\langle q_{1x}\rangle_l^+ + \langle\gamma_{11ss}\rangle\langle q_{1x}\rangle_s^+$$
$$+ \langle\tau_{21fs}\rangle\langle q_{2x}\rangle_f^- + \langle\tau_{21ls}\rangle\langle q_{2x}\rangle_l^- + \langle\tau_{21ss}\rangle\langle q_{2x}\rangle_s^-,$$

$$\langle q_{2x}\rangle_f^+ = \langle\tau_{12ff}\rangle\langle q_{1x}\rangle_f^+ + \langle\tau_{12lf}\rangle\langle q_{1x}\rangle_l^+ + \langle\tau_{12sf}\rangle\langle q_{1x}\rangle_s^+$$
$$+ \langle\gamma_{22ff}\rangle\langle q_{2x}\rangle_f^- + \langle\gamma_{22lf}\rangle\langle q_{2x}\rangle_l^- + \langle\gamma_{22sf}\rangle\langle q_{2x}\rangle_s^-,$$

$$\langle q_{2x}\rangle_l^+ = \langle\tau_{12fl}\rangle\langle q_{1x}\rangle_f^+ + \langle\tau_{12ll}\rangle\langle q_{1x}\rangle_l^+ + \langle\tau_{12sl}\rangle\langle q_{1x}\rangle_s^+ \quad \text{and}$$
$$+ \langle\gamma_{22fl}\rangle\langle q_{2x}\rangle_f^- + \langle\gamma_{22ll}\rangle\langle q_{2x}\rangle_l^- + \langle\gamma_{22sl}\rangle\langle q_{2x}\rangle_s^-,$$

$$\langle q_{2x}\rangle_s^+ = \langle\tau_{12fs}\rangle\langle q_{1x}\rangle_f^+ + \langle\tau_{12ls}\rangle\langle q_{1x}\rangle_l^+ + \langle\tau_{12ss}\rangle\langle q_{1x}\rangle_s^+$$
$$+ \langle\gamma_{22fs}\rangle\langle q_{2x}\rangle_f^- + \langle\gamma_{22ls}\rangle\langle q_{2x}\rangle_l^- + \langle\gamma_{22ss}\rangle\langle q_{2x}\rangle_s^-. \tag{15a-f}$$

Like the previous one-dimensional problem, the reverberance factor ($\Re_m = \psi_m L$) of "m"-type wave field in a two-dimensional subsystem can be defined by ψ_m multiplied by the characteristic length of the subsystem L. If the reverberance factors of plates are small, the hybrid boundary condition for plate structures can be derived because the value of boundary can represent the averaged value of one subsystem. Therefore, the power per unit length of the line junction which is transferred from plates 1 to 2 can be expressed by equation (16), using the coupling loss factor of SEA,

$$\Pi_{1m \to 2n} = \frac{\omega S_1 \eta_{12mn}\langle e_1\rangle_m}{L}, \tag{16}$$

where S_1 is the area of plate 1, η_{12mn} is the coupling loss factor from the energy of a "m"-type wave in plate 1 to a "n"-type wave in plate 2, L is the length of the line junction, and $\langle e_1\rangle_m$ is the energy density (J/m^2) of the "m"-type wave in plate 1. Here, the coupling loss factor of line junction in the plate is known as

$$\eta_{12mn} = \frac{c_{g1m} \cdot L \cdot \langle \tau \rangle_{12mn}}{\omega \pi S_1}, \tag{17}$$

where c_{g1m} is the group velocity of the "m"-type wave in plate 1, L is the length of line junction among plates, and S_1 is the area of plate 1. Using equations (14), (16) and (17), the net power of the "m"-type wave from plates 1 to 2 is represented as

$$\Pi_{1m2n} = -\frac{c_{g1m}^2}{\eta_1 \omega}\nabla\langle e\rangle_{1m} \cdot \vec{n} = \sum_{n=f,l,s}(\Pi_{1m\to 2n}-\Pi_{2n\to 1m})$$

$$= \sum_{n=f,l,s}\frac{\omega}{L}(S_1\eta_{12mn}\langle e_1\rangle_m - S_2\eta_{21mn}\langle e_2\rangle_n) \quad \text{and} \tag{18}$$

$$\Pi_{1n2m} = -\frac{c_{g2m}^2}{\eta_2 \omega}\nabla\langle e\rangle_{2m} \cdot \vec{n} = \sum_{n=f,l,s}(\Pi_{1n\to 2m}-\Pi_{2m\to 1n})$$

$$= \sum_{n=f,l,s}\frac{\omega}{L}(S_1\eta_{12mn}\langle e_1\rangle_n - S_2\eta_{21mn}\langle e_2\rangle_m) \tag{19}$$

2.2.1. Numerical examples
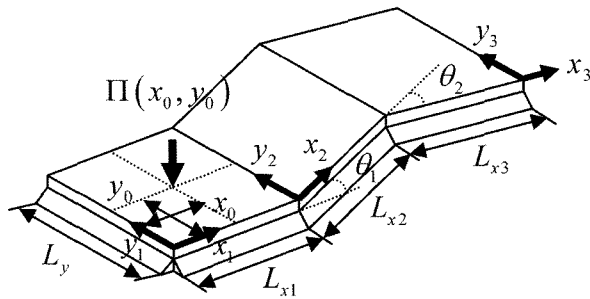The numerical applications of hybrid method for the

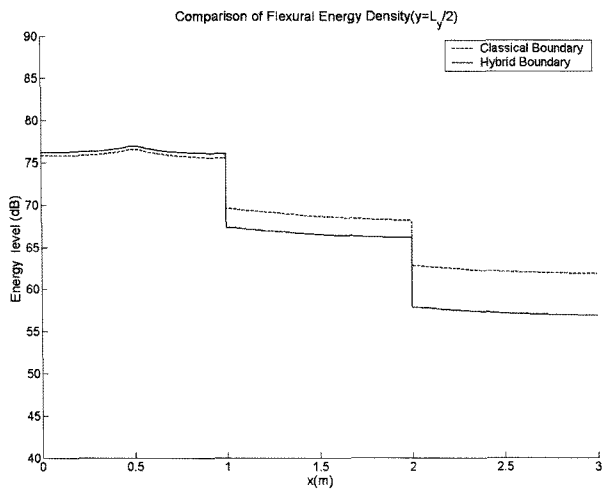Figure 12. Three finite plates joined at arbitrary angles.

Figure 13. The comparison of flexural energy density using the classical and hybrid boundary conditions when $f = 5$ kHz and $\eta = 0.01$.

two-dimensional case are performed for three finite rectangular isotropic plates joined at arbitrary angles and excited by a transverse harmonic point force, as shown in Figure 12. The dimensions and thickness of the structure are $L_{x1}=L_{x2}=L_{x3}=L_y=1m$ and $h = 1$ mm, respectively, and the material properties of the structure are assumed to be the same as those of aluminum ($E=7.1 \times 10^{10}$Pa, $\rho=2700$ kg/m^3). The transverse force is located at $x_0=L_{x1}/2$ and $y_0=L_y/2$ in plate 1 and its amplitude is $F=1$ N. The angles θ_1 and θ_2 between two plates are 90° and −90° respectively.

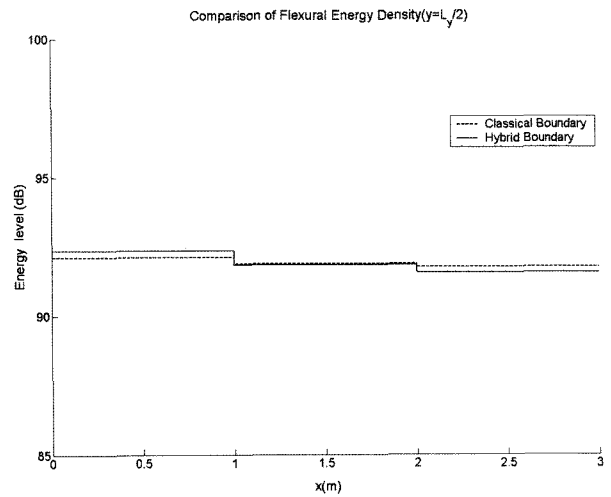
Figure 14. The comparison of flexural energy density using the classical and hybrid boundary conditions when $f = 5$ kHz and $\eta = 0.0001$.
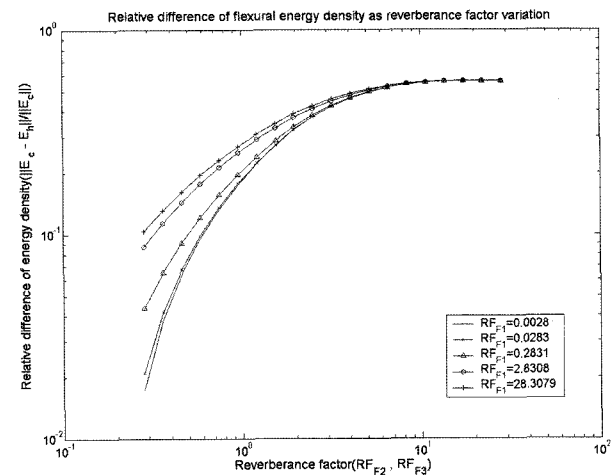

Figure 15. Relative difference ($\|\overline{E_c} - \overline{E_h}\|/\|\overline{E_c}\|$) of space-averaged flexural energy densities by two methods in plate 3 as the reverberance factor variation of plate 1. '——', $\Re_{f1}=1.0028$; '− × −'; $\Re_{f1}=1.028$; '− △ −', $\Re_{f1}=0.28$; '− ○ −', $\Re_{f1}=2.8$; '−|−', $\Re_{f1}=28$.
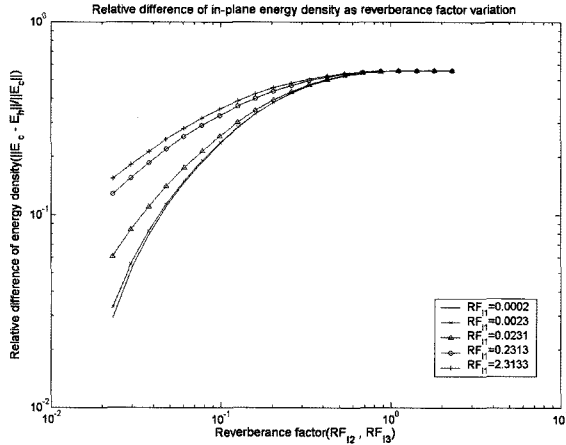
Figure 16. Relative difference ($\|\bar{E}_c - \bar{E}_h\| / |\bar{E}_c|$) of space-averaged in-plane energy densities by two methods in plate 3 as the reverberance factor variation of plate 1. '——', $\mathfrak{R}_{f1} = 0.0002$, '- × -'; $\mathfrak{R}_{f1} = 0.002$; '- △ -', $\mathfrak{R}_{f1} = 0.02$; '- ○ -', $\mathfrak{R}_{f1} = 0.2$; '-|-', $\mathfrak{R}_{f1} = 2$.

The detailed procedure of numerical analysis for the two-dimensional case is discussed in Appendix 2.

Figures 13 and 14 show the comparison of the power flow solutions between those obtained by using the classical and hybrid boundary conditions in $\eta = 0.01$ ($\mathfrak{R}_f = 1.001$, $\mathfrak{R}_l = 8.18 \times 10^{-2}$, $\mathfrak{R}_s = 1.41 \times 10^{-1}$) and $\eta = 0.0001$ ($\mathfrak{R}_f = 1.00 \times 10^{-2}$, $\mathfrak{R}_l = 8.18 \times 10^{-4}$, $\mathfrak{R}_s = 1.41 \times 10^{-3}$), respectively. These figures show that the hybrid boundary condition is equivalent to the classical one for small reverberance factor.

Figures 15 and 16 definitely show the effects of reverberance factors of each plate in the hybrid boundary condition, by using the hybrid boundary condition at all joints. The results in Figures 15 and 16 are the relative differences ($\|\bar{E}_{3,classic} - \bar{E}_{3,hybrid}\| / \|\bar{E}_{3,classic}\|$) of space-averaged flexural and longitudinal energy densities of plate 3 using the classical and hybrid boundary conditions for various structural damping values, respectively. Like the one-dimensional case, as the reverberance factors of plates decrease, the energy density levels using two boundary conditions become equal.

2.3. Three-dimensional Case

To extend the scope of the application of hybrid boundary condition, the acoustic wave in enclosures will be considered as the three-dimensional problem. Bouthier et al. (1992) found the second-order energy differential equation for the propagation of acoustic waves in damped medium,

$$\frac{c_{ga}^2}{\eta\omega}\left(\frac{\partial^2}{\partial x^2} + \frac{\partial^2}{\partial y^2} + \frac{\partial^2}{\partial z^2}\right)\langle e\rangle_a + \eta\omega\langle e\rangle_a = \Pi_{in,a}, \tag{20}$$

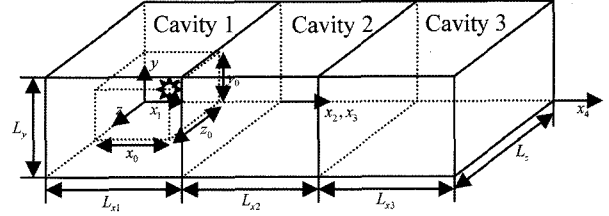where $\langle e\rangle_a$ is the time- and locally space-averaged far-

Figure 17. Acoustic cavities joined without partitions.

field acoustic energy density, and $\Pi_{in,a}$ is the power injected by a sound source. The damping loss factor in an acoustic medium is defined as

$$\eta = \omega\tau, \tag{21}$$

where τ is the relaxation time. The relaxation time models the delay between the application of a sudden pressure change and the resulting equilibrium condensation. The time- and locally space-averaged far-field acoustic intensity is related to the time- and locally space-averaged far-field acoustic energy density by

$$\langle \vec{I}\rangle_a = \frac{c_{ga}^2}{\eta\omega}\left(\frac{\partial}{\partial x}\vec{i} + \frac{\partial}{\partial y}\vec{j} + \frac{\partial}{\partial z}\vec{k}\right)\langle e\rangle_a, \tag{22}$$

where c_{ga} is the group velocity for acoustic waves in gases. The group velocity for acoustic waves is same as the phase speed and is given by

$$c_{ga} = c = \sqrt{\frac{\gamma P_0}{\rho_0}}, \tag{23}$$

where γ is the ratio of the specific heats of the gas at constant pressure to the specific heat of the gas at constant volume, P_0 is the standard pressure, and ρ_0 is the density of various gases (Cho, 1993). Figure 17 shows the power flow model for three acoustic cavities of different acoustic properties. In the model shown in Figure 17, regardless of the acoustic reverberance, the classical boundary conditions of power flow solutions for acoustic wave, which is used in classical power flow analysis, can be expressed as

$$\langle q\rangle_{a2,x}^+ = \tau_{12}\langle q\rangle_{a1,x}^+ + \gamma_{22}\langle q\rangle_{a2,x}^+ \text{ and} \tag{24a}$$

$$\langle q\rangle_{a1,x}^+ = \gamma_{11}\langle q\rangle_{a1,x}^+ + \tau_{21}\langle q\rangle_{a2,x}^+, \tag{24b}$$

where $\langle q\rangle_{a,x}^+$ is the intensity of the acoustic wave in the $+x$ -direction and τ and γ are the diffuse power transmission and reflection coefficients of acoustic waves, respectively. Here, the same assumption as the previous cases can be applied. Because the damping loss value of real acoustic medium is very small ($\eta \ll 1$) like that of the air ($O(10^{-4})$), the energy density does not vary greatly in a small acoustic cavity. Therefore, like the previous cases, except for the case that the cavity was loaded acoustically, the assumption that the energy density field in an acoustic cavity is reverberant ($\langle e\rangle =$

Acoustic Energy Density along the plane z=0.5L_z

(a)

Acoustic Energy Density along the plane z=0.5L_z

(b)

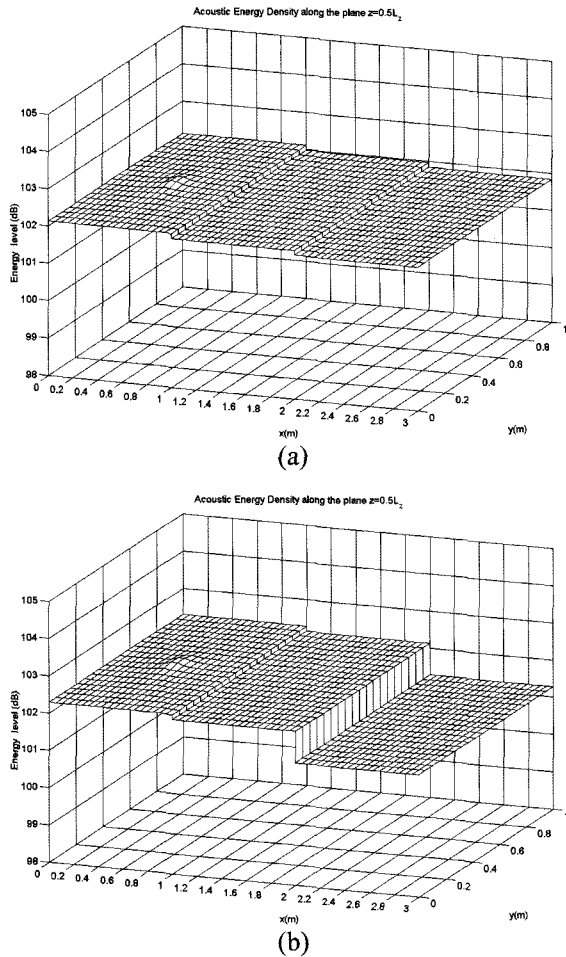Figure 18. Acoustic energy density levels along the plane $z = 0.5L_z$ when $f = 5$ kHz, $\eta_1 = 0.001$ and $\eta_2 = \eta_3 = 0.0005$: (a) Using the classical boundary condition at all area junctions; (b) Using the hybrid boundary condi-tion only at $x = 2m$.

constant) will be reasonable. If the energy density field in each acoustic cavity is assumed to be reverberant, the power per unit area transferred from the energy of acoustic waves in cavities 1 to 2 can be expressed as equation (25), which uses the coupling loss factor of SEA,

$$\Pi_{1a \rightarrow 2a} = \frac{\omega V_1 \eta_{12} \langle e_1 \rangle_a}{S}, \tag{25}$$

where V_1 is the volume of acoustic cavity 1, η_{12} is the coupling loss factor from cavities 1 to 2, S is the area of area junction between acoustic cavities, and $\langle e_1 \rangle_a$ is the energy density (J/m^3) of acoustic wave in cavity 1. The coupling loss factor for area junction in acoustic cavities is known as

$$\eta_{12} = \frac{c_{g1a} \cdot S \cdot \langle \tau \rangle_{12}}{4 \omega V_1} \tag{26}$$

where $\langle \tau \rangle_{12}$ is the diffuse sound power transmission coefficient between cavities 1 and 2. The net power of the acoustic wave from cavities 1 to 2 using equations (22) and (25) and the coupling loss factor may be represented as follows:

$$\Pi_{12} = (\Pi_{1 \rightarrow 2} - \Pi_{2 \rightarrow 1})$$

$$= \frac{c_{g1a}^2}{\eta_1 \omega} \nabla \langle e \rangle_{1a} \cdot \vec{n} = \frac{c_{g2a}^2}{\eta_2 \omega} \nabla \langle e \rangle_{2a} \cdot \vec{n} \tag{27}$$

$$= \frac{\omega}{S} (V_1 \eta_{12} \langle e_1 \rangle_a - V_2 \eta_{21} \langle e_2 \rangle_a).$$

Numerical examples

The numerical applications of hybrid method for the three-dimensional case are performed for coupled three acoustic cavities, as shown in Figure 17. Each cavity has the same dimension of $L_{x1} = L_{x2} = L_{x3} = L_y = L_z = 1$m. The acoustic properties of each cavity were assumed to be $\rho_1 = 1.3$ kg/m³, $c_1 = 330$ m/s, $\rho_2 = 1.35$ kg/m³, $c_2 = 340$ m/s and $\rho_3 = 1.37$ kg/m³, $c_3 = 350$ m/s. Acoustic power is input at $x_0 = L_{x1}/2$, $y_0 = L_y/2$ and $z_0 = L_z/2$ in cavity 1 and its magnitude is $P = 1W$. The detail procedure of numerical analysis is discussed in Appendix 3. Figure 18 shows three-dimensional power flow solutions along the plane $z = 0.5L_z$ when the exciting frequency is $f = 5$ kHz. Figure 18(a) is the power flow solution using the classical boundary condition given in equation (24) in all area junctions and Figure 18(b) is that using the hybrid boundary condition given in equation (27) only in the junction of $x = 2m$. In both solutions, acoustic damping loss factors of cavities 1, 2 and 3 were assumed to be $\eta_1 = 0.001$ and $\eta_2 = \eta_3 = 0.0005$, respectively.

Therefore, the reverberance factors of each acoustic cavity are $\Re_{a1} = 1.6489$, $\Re_{a2} = 0.16$ and $\Re_{a3} = 0.1555$. The diffuse acoustic power transmission and reflection coefficients used in two area junctions are evaluated numerically.

As expected, in Figure 18, the acoustic input power in both cases using each boundary condition propagates well from cavities 1 to 3, with spatial variation of energy. In addition, the difference of energy densities by each solution in cavity 3 is about 0.4dB at maximum due to small reverberance factors. The effects of reverberance factors of acoustic cavity in the hybrid boundary condition are confirmed by the relative difference between space-averaged acoustic energy densities of cavity 3 under the classical and hybrid boundary conditions as the reverberance factor variation of cavities 2 and 3. In Figure 19, the hybrid boundary condition is applied only in the area junction between cavities 2 and 3. Similar to the previous cases, according as the reverberance factor decreases, the power flow solutions using two boundary conditions become equivalent.
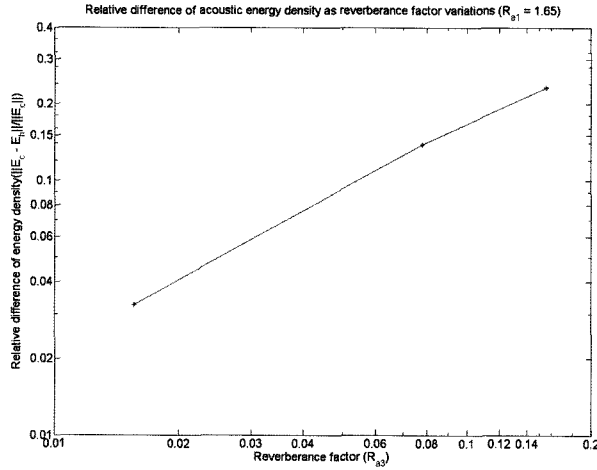
Figure 19. Relative difference ($\|\bar{E_c} - \bar{E_h}\| / |\bar{E_c}|$) between space-averaged acoustic energy densities of cavity 3, using the classical and hybrid boundary conditions as the reverberance factor variation of cavities 2 and 3 in $\Re_{a1} = 1.65$.

3. HYBRID POWER FLOW FINITE ELEMENT METHOD

3.1. Hybrid Boundary Condition for PFFEM

For power flow analysis of built-up structures, the numerical approach for energy governing equation is required. Cho (1993) presented the finite element formulation for the one-dimensional energy equation by considering multi degrees-of-freedoms and two-dimensional energy equation by considering one degree-of-freedom. Seo *et al.*(2000) expanded into the general finite element formulation for two-dimensional case. Seo and Park (2003) developed the software for vibration analysis, PFADS (Power Flow Analysis Design System), based on PFFEM. This paper represents the general hybrid power flow finite element formulation using coupling loss factor in SEA. As known, to apply the hybrid boundary condition to PFFEM, the derivation of new joint element matrix used for linearization of the global matrix equation in PFFEM is required.

To develop the hybrid power flow finite element formulation of two-dimensional energy equation, the weak variational form of the energy governing equation for the propagation of "m"-type wave is obtained and by Galerkin weighted residual method, the following equation is obtained;

$$\sum_{j=1}^{n}\left\{\int_{D}\left(\frac{c_{gm}^2}{\eta\omega}\nabla\phi_i \cdot \nabla\phi_j + \eta\omega\phi_i\phi_j\right)dD\right\}e_j$$

$$= \int_{D}\Pi_m\phi_i dD + \int_{\Gamma}\phi_i\left\{(-n) \cdot \left\langle\vec{I}\right/_m\right\}d\Gamma, \tag{28}$$

where ϕ_i is the basis function for energy approximation

($\langle e\rangle_m = \sum_{j=1}^{n}e_j\phi_j$), n is a unit vector normal to the domain boundary Γ and the "m"-type intensity in the boundary

is $\left\langle\vec{I}\right/_m = -c_{gm}^2\nabla\langle e\rangle_m / \eta\omega$. Equation (28) can be written in element matrix form as

$$[K^{(e)}]\{e^{(e)}\} = \{F^{(e)}\} + \{Q^{(e)}\}, \tag{29}$$

where

$$K_{m,ij}^{(e)} = \int_{D}\left(\frac{c_{gm}^2}{\eta\omega}\nabla\phi_i \cdot \nabla\phi_j + \eta\omega\phi_i\phi_j\right)dD,$$

$$F_{m,i}^{(e)} = \int_{D}\Pi_m\phi_i dD \text{ and}$$

$$Q_{m,i}^{(e)} = \int_{\Gamma}\phi_i\left\{(-n) \cdot \left\langle\vec{I}\right/_m\right\}d\Gamma.$$

The negative sign of $Q_{m,i}^{(e)}$ term means the net power flux of the inner-direction of element. When element matrix equations of all elements are acquired, the global matrix equation has to be assembled to solve the linear equation. The global matrix equation for two-dimensional cases can be represented as

$$[K]\{e\} = \{F\} + \{Q\}. \tag{30}$$

First of all, if the only terms about one degree-of-freedom are considered, the matrix $\{Q\}$, a global power flow matrix, includes the differential terms of energy density and can be expanded to

$$\{Q_m\} = \{\cdots, Q_m^{(k)}, Q_m^{(k+1)}, \cdots\}^T, \tag{31}$$

where

$$Q_m^{(k)} = \{Q_{m1}^{(k)}, \cdots, Q_m^{(k)}\}$$

$$= \left\{\int_{\Gamma_k}\phi_1^{(k)}q_m^{(k)} d\Gamma_k, \cdots, \int_{\Gamma_k}\phi_n^{(k)}q_m^{(k)}d\Gamma_k\right\} \text{ and} \tag{32}$$

$$Q_m^{(k+1)} = \{Q_{m1}^{(k+1)}, \cdots, Q_{mn}^{(k+1)}\}$$

$$= \left\{\int_{\Gamma_{k+1}}\phi_1^{(k+1)}q_m^{(k+1)} d\Gamma_{k+1}, \cdots, \int_{\Gamma_{k+1}}\phi_n^{(k+1)}q_m^{(k+1)}d\Gamma_{k+1}\right\}. \tag{33}$$

In equations (32) and (33), $Q_m^{(k)}$ and $Q_m^{(k+1)}$ are the "m'-type boundary energy flux vectors of for two adjacent boundary elements, k and $k+1$, lying on the line joint of two elements. Here, considering the hybrid boundary condition given in equations (18) and (19), the joint energy flow equations can be expressed as, using coupling loss factor in SEA,
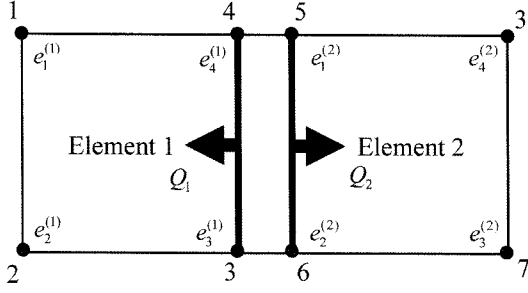
Figure 20. Two 4-node quadrilateral elements for hybrid power flow finite element method.

$$q_m^{(k)} = P_{(k+1)(k)} - P_{(k)(k+1)}$$

$$= \frac{\omega}{L^2}\{-S_{(k)}\eta_{(k)(k+1)mm}e_m^{(k)} + S_{(k+1)}\eta_{(k+1)(k)mm}e_m^{(k+1)}\} \quad \text{and}$$

(34)

$$q_m^{(k+1)} = P_{(k)(k+1)} - P_{(k+1)(k)}$$

$$= \frac{\omega}{L^2}\{S_{(k)}\eta_{(k)(k+1)mm}e_m^{(k)} - S_{(k+1)}\eta_{(k+1)(k)mm}e_m^{(k+1)}\},$$

(35)

where $e_{m,j}^{(k)}$ is the nodal value of "m"-type energy in the boundary element k, $S_{(k)}$ is the area of the element including boundary element k, L is the total length of line junction and $\eta_{(k)(k+1)mm}$ is the coupling loss factor between "m"-type energies of the element including boundary elements k and $k+1$.

The values of energy density in the boundary element can be approximated by

$$e_m^{(k)} = \sum_{j=1}^{n}\phi_j e_{mj}^{(k)},$$

(36)

where $e_{mj}^{(k)}$ are nodal values of "m"-type energy density of the boundary element, ϕ_j are the basis function, and the integer n, is the number of the basis function.

$$\begin{Bmatrix} \vdots \\ Q_m^{(k)} \\ Q_m^{(k+1)} \\ \vdots \end{Bmatrix} = \frac{\omega}{L^2}\begin{bmatrix} \vdots \\ -S_{(k)}\eta_{(k)(k+1)mm}\sum_{j=1}^{n}\left(e_{mj}^{(k)}\oint_{\Gamma}\phi_i\,\phi_j d\Gamma\right) + S_{(k+1)}\eta_{(k+1)(k)mm}\sum_{j=1}^{n}\left(e_{mj}^{(k+1)}\oint_{\Gamma}\phi_i\,\phi_j d\Gamma\right) \\ S_{(k)}\eta_{(k)(k+1)mm}\sum_{j=1}^{n}\left(e_{mj}^{(k)}\oint_{\Gamma}\phi_i\,\phi_j d\Gamma\right) - S_{(k+1)}\eta_{(k+1)(k)mm}\sum_{j=1}^{n}\left(e_{mj}^{(k+1)}\oint_{\Gamma}\phi_i\,\phi_j d\Gamma\right) \\ \vdots \end{bmatrix}$$

(37)

To illustrate the global matrix assembly procedure, the example shown in Figure 20 is considered. In Figure 20, the global nodes are not real finite element nodes. In a common finite element model, the model composed of two coupled quadrilateral elements is modeled with six nodes. However, because the discontinuity of energy density occurs in the coupled line junction, two virtual nodes have to be added in PFFEM and the numbers of total nodes are renumbered as shown in Figure 20. In case of the example shown in Figure 20, equation (37) can be expressed as, with the nodal values of the

boundary nodes, that is, nodes 3, 4, 6 and 5,

$$\begin{Bmatrix} Q_{m3} \\ Q_{m4} \\ Q_{m6} \\ Q_{m5} \end{Bmatrix} = \frac{\omega l}{L^2}\begin{bmatrix} -S_1\eta_{12mm}\begin{bmatrix}1/3 & 1/6\\1/6 & 1/3\end{bmatrix}\begin{Bmatrix}e_{m3}^{(1)}\\e_{m4}^{(1)}\end{Bmatrix} + S_2\eta_{21mm}\begin{bmatrix}1/3 & 1/6\\1/6 & 1/3\end{bmatrix}\begin{Bmatrix}e_{m2}^{(2)}\\e_{m1}^{(2)}\end{Bmatrix} \\ S_1\eta_{12mm}\begin{bmatrix}1/3 & 1/6\\1/6 & 1/3\end{bmatrix}\begin{Bmatrix}e_{m3}^{(1)}\\e_{m4}^{(1)}\end{Bmatrix} - S_2\eta_{21mm}\begin{bmatrix}1/3 & 1/6\\1/6 & 1/3\end{bmatrix}\begin{Bmatrix}e_{m2}^{(2)}\\e_{m1}^{(2)}\end{Bmatrix} \end{bmatrix} = [J]\begin{Bmatrix} e_{m3} \\ e_{m4} \\ e_{m6} \\ e_{m5} \end{Bmatrix},$$

(38)

where l is the length of line junction between elements.

To consider the case of full degree-of-freedoms in the plate, equation (37) can be expanded into

$$\begin{Bmatrix} \vdots \\ Q_f^{(k)} \\ Q_l^{(k)} \\ Q_s^{(k)} \\ Q_f^{(k+1)} \\ Q_l^{(k+1)} \\ Q_s^{(k+1)} \\ \vdots \end{Bmatrix} = \frac{\omega}{L^2}\begin{bmatrix} \vdots \\ -S_{(k)}\left\{\sum_{p=f,l,s}(\eta_{(k)(k+1)fp})\right\}\left\{\sum_{j=1}^{n}\left(e_{f,j}^{(k)}\oint_{\Gamma}\phi_i\,\phi_j d\Gamma\right)\right\} + S_{(k+1)}\left\{\sum_{p=f,l,s}\left(\eta_{(k+1)(k)fp}\right)\left\{\sum_{j=1}^{n}\left(e_{p,j}^{(k+1)}\oint_{\Gamma}\phi_i\,\phi_j d\Gamma\right)\right\}\right\} \\ S_{(k)}\left\{\sum_{p=f,l,s}\eta_{(k)(k+1)lp}\left\{\sum_{j=1}^{n}\left(e_{p,j}^{(k)}\oint_{\Gamma}\phi_i\,\phi_j d\Gamma\right)\right\}\right\} - S_{(k+1)}\left\{\sum_{p=f,l,s}(\eta_{(k+1)(k)lp})\right\}\left\{\sum_{j=1}^{n}\left(e_{p,j}^{(k+1)}\oint_{\Gamma}\phi_i\,\phi_j d\Gamma\right)\right\} \\ -S_{(k)}\left\{\sum_{p=f,l,s}(\eta_{(k)(k+1)sp})\right\}\left\{\sum_{j=1}^{n}\left(e_{s,j}^{(k)}\oint_{\Gamma}\phi_i\,\phi_j d\Gamma\right)\right\} + S_{(k+1)}\left\{\sum_{p=f,l,s}\eta_{(k+1)(k)sp}\left\{\sum_{j=1}^{n}\left(e_{p,j}^{(k+1)}\oint_{\Gamma}\phi_i\,\phi_j d\Gamma\right)\right\}\right\} \\ S_{(k)}\left\{\sum_{p=f,l,s}\eta_{(k)(k+1)fp}\left\{\sum_{j=1}^{n}\left(e_{p,j}^{(k)}\oint_{\Gamma}\phi_i\,\phi_j d\Gamma\right)\right\}\right\} - S_{(k+1)}\left\{\sum_{p=f,l,s}(\eta_{(k+1)(k)fp})\right\}\left\{\sum_{j=1}^{n}\left(e_{p,j}^{(k+1)}\oint_{\Gamma}\phi_i\,\phi_j d\Gamma\right)\right\} \\ -S_{(k)}\left\{\sum_{p=f,l,s}(\eta_{(k)(k+1)lp})\right\}\left\{\sum_{j=1}^{n}\left(e_{s,j}^{(k)}\oint_{\Gamma}\phi_i\,\phi_j d\Gamma\right)\right\} + S_{(k+1)}\left\{\sum_{p=f,l,s}\eta_{(k+1)(k)lp}\left\{\sum_{j=1}^{n}\left(e_{p,j}^{(k+1)}\oint_{\Gamma}\phi_i\,\phi_j d\Gamma\right)\right\}\right\} \\ S_{(k)}\left\{\sum_{p=f,l,s}\eta_{(k)(k+1)sp}\left\{\sum_{j=1}^{n}\left(e_{p,j}^{(k)}\oint_{\Gamma}\phi_i\,\phi_j d\Gamma\right)\right\}\right\} - S_{(k+1)}\left\{\sum_{p=f,l,s}(\eta_{(k+1)(k)sp})\right\}\left\{\sum_{j=1}^{n}\left(e_{s,j}^{(k+1)}\oint_{\Gamma}\phi_i\,\phi_j d\Gamma\right)\right\} \\ \vdots \end{bmatrix}.$$

(39)

where $\eta_{(k)(k+1)mp}$ is coupling loss factor from the "m"-type energy in the boundary element k to the "p"-type energy in the boundary element $k+1$. Using equation (39), equation (38) can be expanded as

$$\begin{Bmatrix} Q_{f} \\ Q_{l} \\ Q_{s} \\ Q_{f} \\ Q_{l} \\ Q_{s} \\ Q_{f} \\ Q_{l} \\ Q_{s} \end{Bmatrix} = \frac{\omega}{L}\begin{bmatrix} -S\left(\sum_{p=f,l,s}\eta_{2fp}\right)[m] & S\eta_{2lf}[m] & 0 & S\eta_{2sf}[m] & 0 & S\eta_{2sf}[m] \\ S\eta_{2fl}[m] & -S\left(\sum_{p=f,l,s}\eta_{2lp}\right)[m] & S\eta_{2sl}[m] & 0 & S\eta_{2sl}[m] & 0 \\ 0 & S\eta_{2fs}[m] & -S\left(\sum_{p=f,l,s}\eta_{2sp}\right)[m] & S\eta_{2ls}[m] & 0 & S\eta_{2ls}[m] \\ S\eta_{2sf}[m] & 0 & S\eta_{2fl}[m] & -S\left(\sum_{p=f,l,s}\eta_{1fp}\right)[m] & S\eta_{1lf}[m] & 0 \\ 0 & S\eta_{2sl}[m] & 0 & S\eta_{1fl}[m] & -S\left(\sum_{p=f,l,s}\eta_{1lp}\right)[m] & S\eta_{1sl}[m] \\ S\eta_{2fs}[m] & 0 & S\eta_{2ls}[m] & 0 & S\eta_{1fs}[m] & -S\left(\sum_{p=f,l,s}\eta_{1sp}\right)[m] \end{bmatrix}\begin{Bmatrix} e_{f3} \\ e_{f4} \\ e_{f6} \\ e_{f5} \\ e_{l3} \\ e_{l4} \\ e_{l6} \\ e_{l5} \\ e_{s3} \\ e_{s4} \\ e_{s6} \\ e_{s5} \end{Bmatrix}$$

(40)

where $[m_1]$ and $[m_2]$ can be represented as $[m_1]=[m_2]=\frac{1}{6}\begin{bmatrix}2 & 1\\1 & 2\end{bmatrix}$ with the length of boundary in element l. Joint element equation (40) can be expressed as simply

$$\begin{Bmatrix} Q_f \\ Q_l \\ Q_s \end{Bmatrix} = [J]\begin{Bmatrix} e_f \\ e_l \\ e_s \end{Bmatrix}.$$

(41)

The global matrix equation can be assembled as

$$\left(\begin{bmatrix} K_f & & \\ & K_l & \\ & & K_s \end{bmatrix} - [J]\right)\begin{Bmatrix} e_f \\ e_l \\ e_s \end{Bmatrix} = \begin{Bmatrix} \Pi_f \\ \Pi_l \\ \Pi_s \end{Bmatrix}.$$
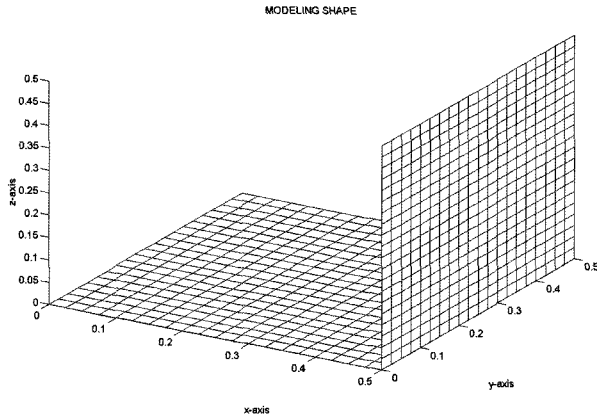
(42)

Figure 21. Finite element model of coupled plates for hybrid PFFEM.

3.2. Numerical Examples

To validate the new joint element formulation for PFFEM using the hybrid boundary condition, the simple model of two coupled plates is applied. The dimensions and thickness of the structure shown in Figure 12 are $L_{x1}=L_{x2}=L_y=0.5$m and $h=10$ mm, respectively, and the material properties of the structure were assumed to be the same as those of aluminum ($E=7.1\times10^{10}$ Pa, $\rho=2700$ kg/m^3). The force position is located at $x_0=L_{x1}/2$ and $y_0=L_y/2$ in plate 1 and its amplitude is $F=100$N. The angle between two plates is 90°. The damping loss factors for all plates were assumed to be 0.01. Figure 21 shows the finite element model of a coupled plate structure for numerical applications. The finite element model shown in Figure 21 has 800 elements, 882 nodes and 2646 dofs. Figure 22 shows the comparison of the analytic power flow results by exact solutions and the numerical power flow results by hybrid PFFEM, respectively, in the line $y = L_y/2$ when $f = 10$ kHz. As expected, the numerical results of hybrid PFFEM agree well with those of the analytic results using the hybrid concept. By these results, the new joint element matrix for hybrid PFFEM was validated successively. Like the tendency in the results of previous examples, as the reverberance factor of structural subsystem decreases, the results of the hybrid power flow finite element solution will become equivalent to those of the classical power flow solution.

Additionally, to expand the application region of hybrid PFFEM to built-up structures, an additional example is presented. Figure 23 shows the finite element model of an automobile-shaped structure, which is composed of 706 nodes, 704 elements and 2616 dofs. The material properties were assumed to be those of steel and the thickness of all plates is 0.001m. Figures 24 and 25 show the analytic results of hybrid PFFEM and classical PFFEM, respectively, when $f = 200$ Hz and $\eta=0.0001$.
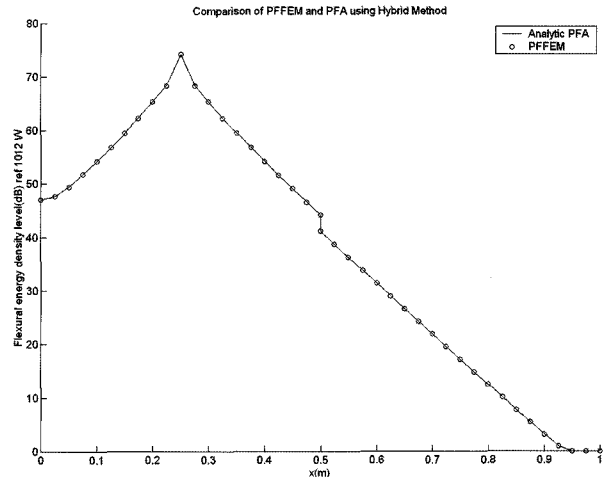
(a)
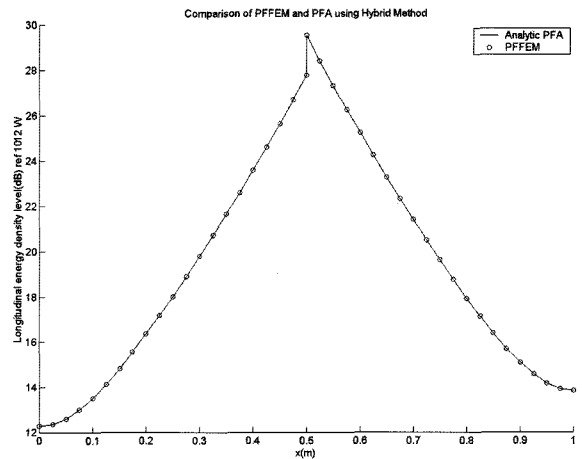
(b)
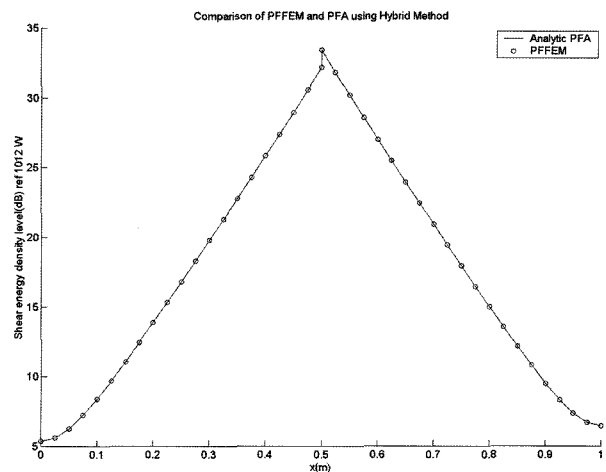
(c)

Figure 22. The comparison of analytic PFA and hybrid PFFEM when 10 kHz and $\eta=0.01$: (a) flexural energy; (b) longitudinal energy; (c) shear energy.
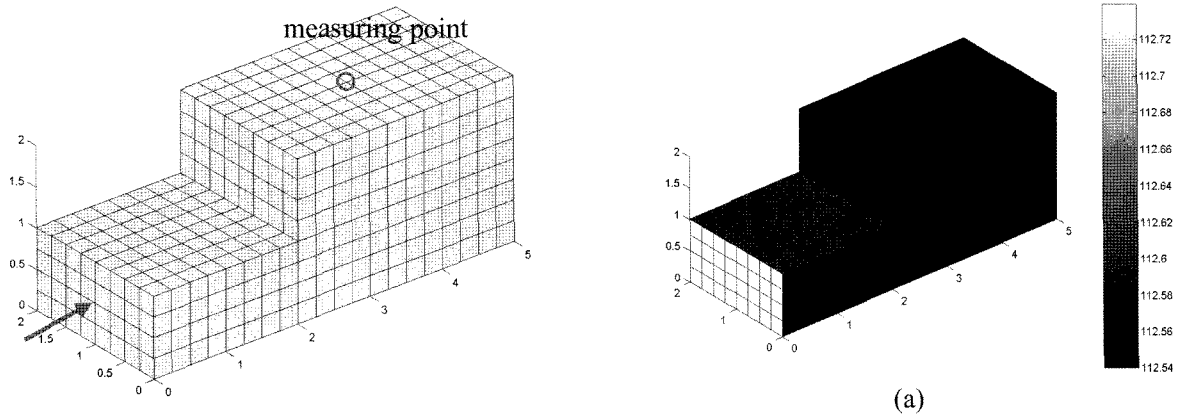
Figure 23. Finite element model of an automobile-shaped structure for hybrid PFFEM.
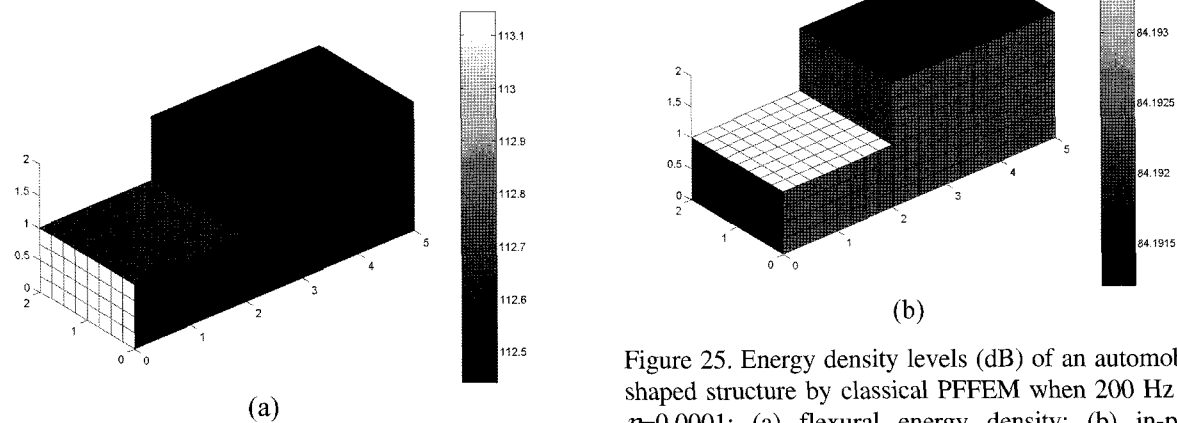

(a)

(b)

Figure 24. Energy density levels (dB) of an automobile-shaped structure by hybrid PFFEM when 200 Hz and $\eta=$ 0.0001: (a) flexural energy density; (b) in-plane energy density.

Additionally, Figures 26 and 27 show the analytic results of hybrid PFFEM and classical PFFEM, respectively, when $f = 500$ Hz and $\eta=0.01$. Since the reverberance factor of Figures 24 and 25 is 250 times as large as that of Figures 26 and 27, the difference between the results of

(a)

(b)

Figure 25. Energy density levels (dB) of an automobile-shaped structure by classical PFFEM when 200 Hz and $\eta=0.0001$: (a) flexural energy density; (b) in-plane energy density.
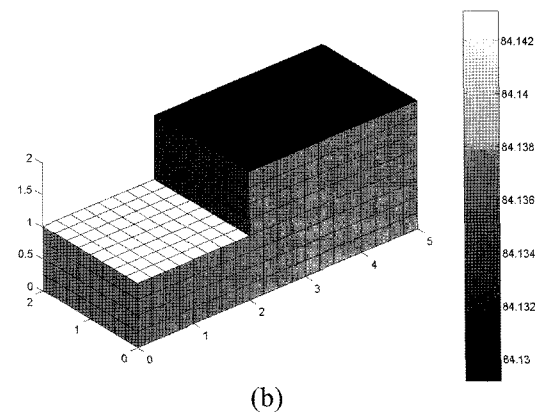
Figures 24 and 25 is much smaller than that between the results of Figures 26 and 27. In Figures 24 and 25, the results of two methods show good agreement and their difference is not more than 1dB. Figure 28 shows the relative difference between classical and hybrid PFFEM in the measuring point shown in Figure 23 as various reverberance factors of the measuring subsystem. Like the previous cases, as the reverberance factor decreases, the results of two methods become equal. Additionally, Figure 29 shows the spatial intensity distributions that cannot be represented in classical SEA. As expected, the hybrid PFFEM for built-up structures is applied successively.

4. CONCLUSION

In this work, the hybrid power flow method using SEA concepts was developed to predict the vibrational and acoustic responses in the medium-to-high frequency ranges for reverberant systems. To develop the general hybrid method which uses SEA parameters in power
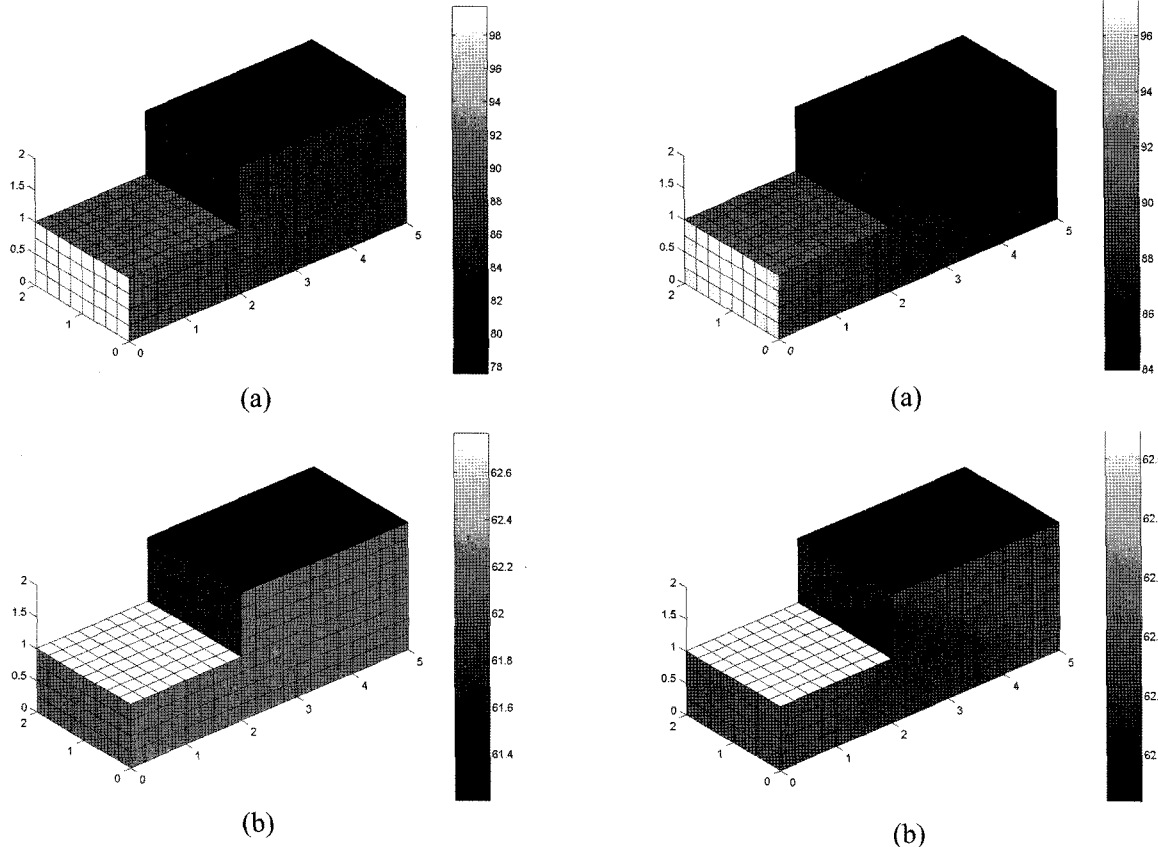
(a)

(b)

Figure 26. Energy density levels (dB) of an automobile-shaped structure by hybrid PFFEM when 500 Hz and $\eta=$ 0.01: (a) flexural energy density; (b) in-plane energy density.

(a)

(b)

Figure 27. Energy density levels (dB) of an automobile-shaped structure by classical PFFEM when 500 Hz and η =0.01: (a) flexural energy density; (b) in-plane energy density.

flow analysis, the general hybrid boundary conditions including all degree-of-freedoms in one-, two-, and three-dimensional cases were derived, and the numerical analyses for the validation of these methods were performed. As a result, the hybrid power flow method was proven to be effective in obtaining power flow solution in the reverberant system. Finally, for the application of the hybrid power flow method to real built-up structures, the new joint element matrix for hybrid PFFEM was derived and was validated by the several successive numerical applications. In the medium-to-high frequency ranges, the developed hybrid power flow method can be an effective tool for the prediction of vibrational and acoustic responses in built-up vehicle structures, such as an automobile, ship and aircraft, especially when it uses experimental data for the reverberant system.
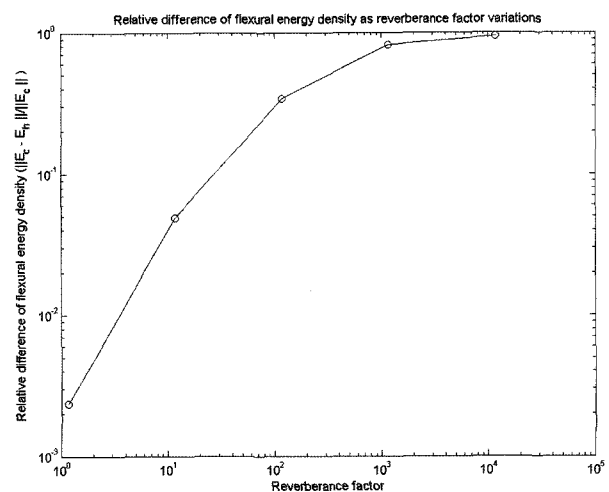
Figure 28. Relative difference ($\|\overline{E}_c - \overline{E}_h\| / |\overline{E}_c|$) between flexural energy densities in the measuring point, using classical and hybrid PFFEM as the reverberance factor variation of the measuring subsystem.
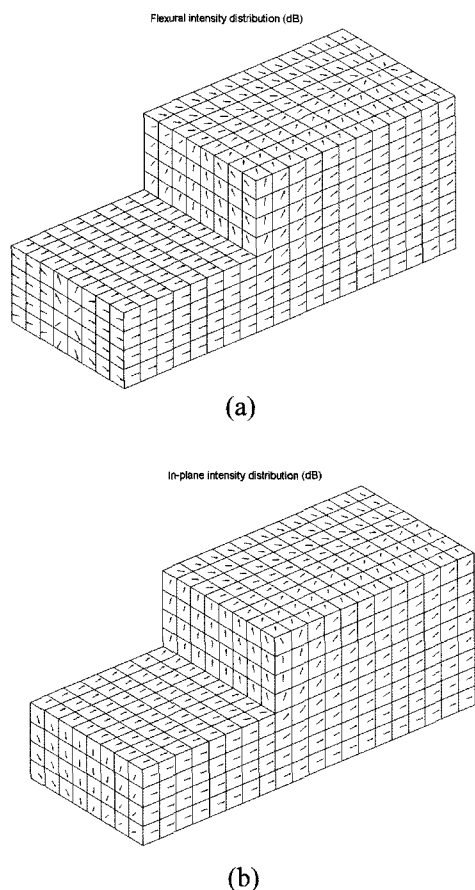
Flexural intensity distribution (dB)

(a)

In-plane intensity distribution (dB)

(b)

Figure 29. Intensity level distributions (dB) of an automobile-shaped structure by hybrid PFFEM when 500 Hz and η=0.01: (a) flexural intensity; (b) in-plane intensity.

REFERENCES

Bouthier, O. H. and Bernhard, R. J. (1992). Models of spaced-averaged energetics of plates. *AIAA J.* **30**, 3, 616–623.

Cho, P. E. (1993). *Energy Flow Analysis of Coupled Structures.* Ph. D. Dissertation. Purdue University.

Chuang, C.-H., Shu, K.-T., Liu, W. and Qian, P. (2005). A CAE optimization process for vehicle high frequency NVH applications. *SAE Noise and Vibration Conf. & Exhibition*, Traverse City, USA.

Goyder, H. G. D. and White, R. G. (1980). Vibrational power flow from machines into built-up structures: Part I. *J. Sound and Vibration*, **68**, 59–75.

Langley, R. S. (1995). On the vibrational conductivity approach to high frequency dynamics for two-dimensional structural components. *J. Sound and Vibration*, **182**, 637–657.

Lyon, R. H. and DeJong, R. G. (1995). *Theory and Application of Statistical Energy Analysis.* 2nd Edn.,

Butterworth-Heinemann, MI, USA.

Manning, P. A. (2005). Energy finite element analysis of a vehicle floor. *SAE Noise and Vibration Conf. & Exhibition*, Traverse City, USA.

Park, D.-H., Hong, S.-Y., Kil, H.-K. and Jeon, J.-J. (2001). Power flow model and analysis of in-plane waves in finite coupled thin plates. *J. Sound and Vibration*, **244**, 651–668.

Park, Y.-H., Hong, S.-Y. and Seo, S.-H. (2003). Development and applications PFA (Power Flow Analysis) software for vibration analysis of auto-mobiles. *SAE Noise and Vibration Conf. & Exhibition*, Traverse City, USA.

Park, Y.-H., Hong, S.-Y. and Seo, S.-H. (2003). Development of PFFEM software – "PFADS R3": (II) applications to vehicle vibration analysis. *Proc. Internoise 2003*, Jeju, Korea.

Seo, S.-H. (2000). *Power Flow Finite Element Method for the Various Plate Structures in Shape.* M.S. Thesis. Seoul National University. Korea.

Seo, S.-H., Hong, S.-Y. and Park, Y.-H. (2003). Development of PFFEM software - "PFADS R3": (I) program structures and functions. *Proc. Internoise 2003*, Jeju, Korea.

Wohlever, J. C. (1988). *Vibrational Power Flow Analysis of Rods and Beams.* M.S. Thesis. Purdue University.

Wohlever, J. C. and Bernhard, R. J. (1992). Mechanical energy flow models of rods and beams. *J. Sound and Vibration*, **153**, 1–19.

Zhang, W. and Raveendra, S. T. (2005). Interior noise prediction based on energy finite element method. *SAE Noise and Vibration Conf. & Exhibition*, Traverse City, USA.

APPENDIX

1. Numerical Analysis for One-dimensional Case

The equation and exact solution of flexural motion in beam i using equation (1) can be represented as, respectively,

$$E_{c,i}I_i\frac{\partial^4 w_i}{\partial x_i^4} + \rho_i S_i\frac{\partial^4 w_i}{\partial t^2} = F_f\delta(x_i - x_0)e^{j\omega t} \text{ and} \quad \text{(A.1)}$$

$$w_i(x_i, t)=(A_i e^{-jk_{fi}x_i} + B_i e^{jk_{fi}x_i} + C e^{-k_{fi}x_i} + D e^{k_{fi}x_i})e^{j\omega t}, \quad \text{(A.2)}$$

where w_i is the transverse displacement of beam i and $k_{fi}=(\omega^2\rho_i S_i/E_{c,i}I_i)^{1/4}$ is the flexural wavenumber of beam i. The equation and exact solution of longitudinal motion in beam i can be expressed as, respectively,

$$E_{c,i}S_i\frac{\partial^2 u_i}{\partial x_i^2} + \rho_i S_i\frac{\partial^2 u_i}{\partial t^2} = F_l\delta(x_1 - x_0)e^{j\omega t} \text{ and} \quad \text{(A.3)}$$

$$u_i(x_i, t)=(M_i e^{-jk_{li}x_i} + N_i e^{jk_{li}x_i})e^{j\omega t}, \quad \text{(A.4)}$$

where u_i is the longitudinal displacement of beam i and is the longitudinal wavenumber of beam i. Because there are a total of 22 unknowns, the boundary conditions of the same number must be enforced to solve the problem. The energy governing equations and energy densities of "m"-type energy in beam p using equations (5) and (6) can be represented as, respectively,

$$-\frac{c_{g,mp}^2}{\eta_{mp}\omega}\frac{d^2\langle e\rangle_{mp}}{dx^2} + \eta_{mp}\omega\langle e\rangle_{mp} = \Pi_{in,mp} \quad \text{and} \quad (A.5)$$

$$\langle e\rangle_{mp} = P_{mp}e^{-\varphi_{mp}} + Q_{mp}e^{\varphi_{mp}}, \quad (A.6)$$

where $\langle e\rangle_{mp}$, $c_{g,mp}$ and η_{mp} is the energy density, group velocity, and damping loss factor of "m"-type in beam p, respectively, and $\varphi_{mp} = \eta_{mp}\omega/c_{mp}$. In case of the power flow solution, a total of sixteen unknowns exist.

2. Numerical Analysis for Two-dimensional Case

The energy governing equations for two-dimensional thin plate given in equation (13) can be expressed as

$$-\frac{c_{g,mj}^2}{\eta_{mj}\omega}\left(\frac{d^2}{dx^2} + \frac{d^2}{dy^2}\right)\langle e\rangle_{mj} + \eta_{mj}\omega\langle e\rangle_{mj} = \Pi_{in,mj}, \quad (A.7)$$

where $\langle e\rangle_{mj}$, $c_{g,mj}$, and η_{mj} are the energy density, group velocity and structural damping loss factor of "m"-type in plate j, respectively. If all y-directional boundaries are simply-supported like the model in Figure 12, the analytic solution of equation (A.7) can be obtained as a single series solution,

$$\langle e\rangle_{mj}(x_j, y) = \sum_{n=0}^{\infty} E_{mj,n}\cos k_n y$$

$$= \sum_{n=0}^{\infty}(A_{mj,n}^+ e^{-\lambda_{mj,n}} + A_{mj,n}^- e^{\lambda_{mj,n}})\cos k_n y, \quad (A.8)$$

where $E_{mj,n}$ is the n'th component of the series solution, equation (A.8), $k_n=(n\pi/L_y)$ and $\lambda_{mj,n}^2=(k_n^2 + (\eta_{mj}\omega/c_{g,mj})^2)$. The intensity of "m"-type wave component in the j'th plate can be obtained by the energy transfer relation, equation (14),

$$\langle q_x\rangle_{mj}(x_j, y) = \sum_{n=0}^{\infty} Q_{xmj,n}\cos k_n y$$

$$= \sum_{n=0}^{\infty}\left\{\left(\frac{c_{g,mj}^2}{\eta_{mj}\omega}\lambda_{mj,n}\right)(A_{mj,n}^+ e^{-\lambda_{mj,n}}-A_{mj,n}^- e^{\lambda_{mj,n}})\cos k_n y\right\} \quad \text{and} \quad (A.9)$$

$$\langle q_x\rangle_{mj}(x_j, y) = \sum_{n=0}^{\infty} Q_{ymj,n}\sin k_n y$$

$$= \sum_{n=0}^{\infty}\left\{\left(\frac{c_{g,mj}^2}{\eta_{mj}\omega}k_n\right)(A_{mj,n}^+ e^{-\lambda_{mj,n}} + A_{mj,n}^- e^{\lambda_{mj,n}})\sin k_n y\right\}, \quad (A.10)$$

where $\langle q_x\rangle_{mj}$ and $\langle q_y\rangle_{mj}$ are the x-and y-components of intensity, $\langle q\rangle_{mj}$.

In addition, the input power can be approximated as,

$$\Pi_m\delta(x-x_0)\delta(y-y_0) = \sum_{n=0}^{\infty}\Pi_{m,n}(x)\cos k_n y, \quad (A.11)$$

where Π_m is the input power of "m"-type component. Here, $\Pi_{m,n}$, the n'th component of Π_m, can be expressed as

$$\Pi_{m,n}=\begin{cases}\dfrac{\Pi_m}{L_y}\delta(x-x_0) & (n=0)\\[2ex]\dfrac{2\Pi_m}{L_y}\cos k_n y_0\delta(x-x_0) & (n\neq 0)\end{cases} \quad (A.12)$$

The six unknowns in each plate's domain exist, and a total of twenty four boundary conditions must be enforced. The intensity of each wave component is zero in the simply-supported boundary and the continuity of energy density and intensity of each wave component in loading position must be enforced. In the line junction of coupled plates, equation (15) is applied in the classical power flow solutions, and equations (18-19) are applied in the hybrid power flow solutions.

3. Numerical analysis three-dimensional case

The energy governing equation for a three-dimensional acoustic cavity given in equation (20) can be expressed as, in each cavity

$$-\frac{c_{g,j}^2}{\eta\omega}\left(\frac{\partial^2}{\partial x^2} + \frac{\partial^2}{\partial y^2} + \frac{\partial^2}{\partial z^2}\right)\langle e\rangle_{a,j} + \eta\omega\langle e\rangle_{a,j}=\Pi_{in,j}(x, y, z), \quad (A.13)$$

where $\langle e\rangle_{a,j}$ is the acoustic energy density in cavity j.

If power transferred in all the y-and z-directional area boundaries of cavities is zero in the model shown in Figure 17, the power flow solution of equation (A.13) can be obtained as, double series solution,

$$\langle e\rangle_{a,j}(x_j, y, z) = \sum_{m=0}^{\infty}\sum_{n=0}^{\infty} E_{j,mn}(x_i)\cos(k_m y)\cos(k_n z)$$

$$= \sum_{m=0}^{\infty}\sum_{n=0}^{\infty}(A_{j,mn}^+ e^{-\lambda_{j,mn}} + A_{j,mn}^- e^{\lambda_{j,mn}})\cos(k_m y)\cos(k_n z), \quad (A.14)$$

where $k_m=m\pi/L_y$, $k_n=m\pi/L_z$, and $\lambda_{j,mn}^2=k_n^2 + k_n^2 + (\eta_j\omega/c_{g,j})^2$. The intensity in the j'th acoustic cavity can be obtained by the energy transfer relation, equation (22),

$$\langle q_x\rangle_j(x_j, y, z) =$$

$$\sum_{m=0}^{\infty}\sum_{n=0}^{\infty}\left\{\left(\frac{c_{g,j}^2}{\eta_j\omega}\lambda_{j,mn}\right)\left(A_{j,mn}^+ e^{-\lambda_{j,mn}} - A_{j,mn}^- e^{\lambda_{j,mn}}\right)\cos k_m y\cos k_n z\right\},$$

$$\langle q_y \rangle_j (x_j, y, z) =$$

$$\sum_{m=0}^{\infty} \sum_{n=0}^{\infty} \left\{ \left(\frac{c_{g,j}^2}{\eta_j \omega} k_m \right) \left(A_{j,mn}^+ e^{-\lambda_{j,mn}} + A_{j,mn}^- e^{\lambda_{j,mn}} \right) \sin k_m y \cos k_n z \right\}$$

and

$$\langle q_z \rangle_j (x_j, y, z) =$$

$$\sum_{m=0}^{\infty} \sum_{n=0}^{\infty} \left\{ \left(\frac{c_{g,j}^2}{\eta_j \omega} k_n \right) \left(A_{j,mn}^+ e^{-\lambda_{j,mn}} + A_{j,mn}^- e^{\lambda_{j,mn}} \right) \cos k_m y \sin k_n z \right\},$$

$$(A.15\text{-}17)$$

where $\langle q_x \rangle_j$, $\langle q_y \rangle_j$ and $\langle q_z \rangle_j$ is the x-, y- and z-components of intensity, $\langle q \rangle_j$.

Like the two-dimensional case, the acoustic input power can be approximated as,

$$\Pi \delta(x - x_0) \delta(y - y_0) \delta(z - z_0)$$

$$= \sum_{m=0}^{\infty} \sum_{n=0}^{\infty} \Pi_{mn}(x) \cos k_m y \cos k_n z, \qquad (A.18)$$

where Π is the acoustic input power. Π_{mn}, the m'th and

n'th components of Π can be expressed as

$$\Pi_{m,n} = \begin{cases} \dfrac{\Pi}{L_y L_z} \delta(y - y_0)\delta(z - z_0) & (m = 0, n = 0) \\[2ex] \dfrac{2\Pi}{L_y L_z} \cos k_n z_0 \delta(y - y_0) & (m = 0, n \neq 0) \\[2ex] \dfrac{2\Pi}{L_y L_z} \cos k_m y_0 \delta(z - z_0) & (m \neq 0, n = 0) \\[2ex] \dfrac{4\Pi}{L_y L_z} \cos k_m y_0 \cos k_n z_0 & (m \neq 0, n \neq 0) \end{cases} \qquad (A.19)$$

Two unknowns in each acoustic cavity's domain exist, and a total of eight boundary conditions must be enforced. The intensities of acoustic wave components are zero in the zero-power boundary, and the continuity of the energy density and intensity of each wave component in the source position must be enforced. In the area junction of coupled acoustic cavities, equation (24) is applied in the classical power flow solutions and equation (27) is applied in the hybrid power flow solutions.